Molecular Cancer

CORRESPONDENCE

Open Access

Joint single-cell genetic and transcriptomic analysis reveal pre-malignant SCP-like subclones in human neuroblastoma

Thale K. Olsen[1,2†], Jörg Otte[1†], Shenglin Mei[3†], Bethel Tesfai Embaie[1], Polina Kameneva[4], Huaitao Cheng[5], Teng Gao[3], Vasilios Zachariadis[5], Ioanna Tsea[1], Åsa Björklund[6], Emil Kryukov[7,8], Ziyi Hou[3], Anna Johansson[6], Erik Sundström[9], Tommy Martinsson[10], Susanne Fransson[10], Jakob Stenman[1], Shahrzad Shirazi Fard[1], John Inge Johnsen[1], Per Kogner[1], Igor Adameyko[11,12], Martin Enge[5*], Peter V. Kharchenko[3,13*†] and Ninib Baryawno[1*†]

Abstract

Background Neuroblastoma (NB) is a heterogeneous embryonal malignancy and the deadliest tumor of infancy. It is a complex disease that can result in diverse clinical outcomes. In some children, tumors regress spontaneously. Others respond well to existing treatments. But for the high-risk group, which constitutes approximately 40% of all patients, the prognosis remains dire despite collaborative efforts in basic and clinical research. While its exact cellular origin is still under debate, NB is assumed to arise from the neural crest cell lineage including multipotent Schwann cell precursors (SCPs), which differentiate into sympatho-adrenal cell states eventually producing chromaffin cells and sympathoblasts.

Methods To investigate clonal development of neuroblastoma cell states, we performed haplotype-specific analysis of human tumor samples using single-cell multi-omics, including joint DNA/RNA sequencing of sorted single cells (DNTR-seq). Samples were also assessed using immunofluorescence stainings and fluorescence in-situ hybridization (FISH).

Results Beyond adrenergic tumor cells, we identify subpopulations of aneuploid SCP-like cells, characterized by clonal expansion, whole-chromosome 17 gains, as well as expression programs of proliferation, apoptosis, and a non-immunomodulatory phenotype.

Conclusion Aneuploid pre-malignant SCP-like cells represent a novel feature of NB. Genetic evidence and tumor phylogeny suggest that these clones and malignant adrenergic populations originate from aneuploidy-prone cells of migrating neural crest or SCP origin, before lineage commitment to sympatho-adrenal cell states. Our findings

†Thale K. Olsen, Jörg Otte and Shenglin Mei contributed equally to this work.

†Peter V. Kharchenko and Ninib Baryawno contributed equally to this work.

*Correspondence:
Martin Enge
martin.enge@ki.se
Peter V. Kharchenko
peter.kharchenko@post.harvard.edu
Ninib Baryawno
n.baryawno@ki.se
Full list of author information is available at the end of the article

expand the phenotypic spectrum of NB cell states. Considering the multipotency of SCPs in development, we suggest that the transformation of fetal SCPs may represent one possible mechanism of tumor initiation in NB with chromosome 17 aberrations as a characteristic element.

Keywords Neuroblastoma, Schwann cell precursors, Childhood cancer, Tumor heterogeneity, Tumor evolution, Clonality, Development, Single-cell sequencing, Multi-omics

Background

Neuroblastoma (NB) is a pediatric extra-cranial neuroendocrine cancer, believed to arise at early prenatal stages from the sympatho-adrenal lineage of the neural crest. It is a complex disease with diverse clinical outcomes. In some children, tumors regress spontaneously while others respond well to treatment. However, for the high-risk group, which constitutes approximately 40% of all patients, clinical outcome remains dire [1].

Key genetic aberrations associated with a poor prognosis include *MYCN* amplification, *TERT* rearrangements, hemizygous 1p and 11q deletions, and segmental 17q gain. Whole-chromosome or segmental copy number variations (CNVs) are common in NB. While whole-chromosome CNVs are associated with favorable prognosis, segmental CNVs of any kind are associated with high-risk disease [1].

NB displays considerable heterogeneity on the transcriptional and cell state level. Like many other cancers which activate and replay developmental mechanisms to attain plasticity, NB retains embryonic features which ultimately promote intratumor heterogeneity and resistance to therapy. The neural crest lineage, from which NB originates, is remarkably flexible and involves several cell fate progenitors and transitions [2, 3].

In humans, neural crest-derived Schwann cell precursors (SCPs) play a crucial role in the development of the sympatho-adrenal system. Migratory neural crest cells settle on developing peripheral nerves and turn into nerve-associated SCPs, which are retained for a considerable time during development, while maintaining neural crest-like multipotency at the nerve niche. Via a 'fork-like' transition, SCPs can give rise to neuroendocrine chromaffin cells or immature sympathoblasts which, in turn, can also differentiate directly into chromaffin cells. Besides adrenergic lineages, neural crest cells can also give rise to parasympathetic and enteric neurons, melanocytes, dental pulp progenitors and mesenchymal cells such as cranial fibroblasts [2].

Histologically, NB consists of proliferative neuroendocrine cells of different cell states such as sympathoblast-like or chromaffin-like tumor cells. The identification of Schwann cells, as part of stroma-rich, well-differentiated tumors, usually indicate a benign tumor biology, such as ganglioneuromas [1, 4]. Schwann cells are believed to be recruited into the tumor where they can acquire a repair-like phenotype and fulfill tumor-inhibiting effects such as neuroblast differentiation or modulate the local immune response via the expression of various cytokines and the upregulation of MHC class I and II molecules [5].

Recent studies have analyzed the transcriptomic heterogeneity of NB and correlated tumor cell state dynamics to fetal developmental trajectories [2, 3, 6–8]. Low-risk NB maps to highly differentiated sympathoblasts whereas high-risk tumor cells align to earlier developmental time points with a less differentiated sympatho-adrenal state [3, 8]. Transcriptomic and epigenetic studies also indicate the presence of a more immature phenotype with mesenchymal-like features [3, 6]. Importantly, a "pure" mesenchymal tumor phenotype, as previously described in cell lines, has not been consistently observed in primary patient samples. Mesenchymal features, as described by super-enhancer profiles in patient material, however, are associated with high-risk disease and therapy resistance [3, 6].

A clear picture of cellular ancestry and genomic abnormalities involved in NB development is still lacking. By performing in-depth, single-cell multi-omics profiling of human NB samples, we answer some of these unresolved questions and reveal an unprecedented resolution of NB tumor evolution and its embryological context, including the discovery of abnormal SCPs, of which some are clonally related to adrenergic tumor cells and potentially pre-malignant.

Results

Cellular heterogeneity in human neuroblastoma

For in-depth characterization of NB cellular heterogeneity, we used single-cell RNA sequencing to characterize tumor samples across various clinical risk groups, ages, and genetic subsets (Fig. 1A, S1A; Table S1). A total of eighteen NB samples were profiled using droplet-based single-cell RNA-seq (scRNA-seq, 10x Genomics Chromium), yielding altogether 86796 high quality cells (Fig. 1A; S1A-D) (see Methods).

To overcome inter-individual variation, samples were integrated using the graph-based *Conos* approach which revealed 18 major cell subpopulations common to most

samples, spanning adrenergic, stromal, and immune compartments (Fig. S1D). The immune populations were recently described in a separate publication (Table S1, see Methods), all non-immune cells of this cohort have not been analyzed before. Among the stromal populations, we observed endothelial cells and well-defined clusters of pericytes and myofibroblasts in close proximity to another mesenchymal cell population of a fibroblast identity expressing *MGP, LUM, OGN* and *COL6A3*. The dominant population of adrenergic tumor cells carried an expected expression signature including *TH, DBH, PHOX2B,* and *CD24* (Table S2; Fig. S1C, D; Fig. S2A) [2]. Surprisingly, mesenchymal and adrenergic cell populations were interconnected by a cell type expressing key neural crest and Schwann lineage markers, such as *SOX10, S100B, ERBB3,* and *PLP1* (Fig. S1D, S2A).

NB is thought to arise during differentiation of neural crest-derived cells into sympatho-adrenal lineages [1–3, 8]. To understand how the observed populations of non-immune NB cells relate to normal adrenal development, we aligned our data with published data sets of human fetal adrenal cells. Joint alignment confirmed close resemblance of adrenergic NB cells to fetal sympathoblasts and to some extent chromaffin cells, while stromal cells were similar to fetal mesenchymal cells (Fig. 1B, S1E; see Methods). The observed NB-associated cells expressing *SOX10* aligned with Schwann cell precursors (SCPs) normally observed in fetal development. This suggests the presence of SCP-like cells in NB tumors transcriptionally mimicking human fetal SCPs.

SCP-like neuroblastoma cells harboring aneuploidy represent putative pre-malignant populations

Next, we applied our recently published *Numbat* algorithm, including all non-immune cells in the analysis. By integrating gene expression, allele, and population-based haplotype information, this strategy allows an enhanced detection of genomic CNVs in scRNAseq data. It can reconstruct the subclonal architecture and tumor phylogeny within each sample, allowing identification of ancestral clones.

CNV analysis revealed specific genomic alterations strongly supported by bulk SNP array data, showing matching profiles with high precision (Fig. S1F, S8A). Adrenergic cells were consistently identified as malignant (Fig. 1C, S1G), whereas pericytes, immune, and endothelial cells were classified as normal without any CNVs detected. We did not detect any distinct subclone of malignant mesenchymal cells (Fig. 1C, S1G), although we cannot rule out the possibility of minor genetic alterations in this population. Strikingly, besides the adrenergic tumor populations, a subfraction of SCP-like cells were also found to carry clonal CNVs. These were detected in the sample NB26, a low-risk sample of a previously untreated primary adrenal tumor with numerical chromosomal aberrations (Fig. S1A).

In this tumor sample, Numbat analysis revealed four distinct clones. Clone 1 reflected non-malignant stromal

(See figure on next page.)

Fig. 1 Multi-omic CNV identification in single neuroblastoma cells reveal complex subclonal architectures and identify abnormal SCP-like populations carrying whole-chromosome gains. **A** Graphical illustration of study design and experimental procedures. **B** Joint alignment of neuroblastoma (10x dataset) and normal fetal adrenal scRNAseq data (GEO accession numbers GSE137804 and GSE147821) is shown, indicating normal fetal cell populations (left panel) and corresponding cell types in the neuroblastoma 10x dataset (right panel). Dashed contour lines indicate positions of NB populations: adrenergic, mesenchymal, and SCP-like cells. **C** Integrative Numbat analysis of non-immune cells from all samples where CNVs were inferred: NB09, NB12, NB13, NB15, NB17, NB24, NB26, and NB34. Left panel: Labelled by cell type. Right panel: Labelled by joint posterior aneuploidy probability ("malignancy score"). Red color indicates high probability of CNVs present, blue color indicates low probability. **D** Heatmap of single-cell CNVs and predicted phylogeny of sample NB26. Phylogeny is shown on the left side of the heatmap. Branch lengths corresponds to number of CNVs; horizontal dashed lines separate predicted clones. Bottom clone (clone 1) represents predicted normal cells. Annotation column to the left indicates subclone, annotated cell type, and predicted CNV state. Chromosomes are ordered along the x axis in increasing order. AMP: amplification (i.e. copy number gain), BAMP: balanced amplification (i.e. expression-based CNV prediction without allelic support), CNLoH: copy number neutral loss of heterozygosity. **E** UMAP embedding of 10x sample NB26, labelled by cell type. **F** UMAP embedding of 10x sample NB26, labelled by subclone. Subclones correspond to those shown in Fig. 1D. **G** CNV identification in DNTR-seq data. Common UMAP embedding of RNA-seq data (samples: $n = 5$) labelled by cell type; initial cluster-based annotation (left panel) or CNV status in DNA data (right panel). All adrenergic cells display multiple CNVs. **H** UMAP embedding of DNTR-seq sample THA004, labelled by cell type. **I** Bar plot showing the fraction of clones per cell type. Clones correspond to those shown in Fig. 1J. **J** Heatmap indicating single-cell CNVs and subclones detected in DNTR-seq sample THA004. Chromosomes are indicated in increasing order along the x axis. Blue color indicates copy number loss, red color indicates copy number gain. Annotation columns to the right indicate cell type, annotated from corresponding RNA-level data, and subclone, where subclone A indicates normal cells (no CNVs detected). **K** Manually reconstructed phylogeny and suggested clonal evolution of samples NB26 and THA004. Each circle indicates one subclone. Circle color indicates cell state. Clones below dashed horizontal line correspond to those who constitute the bulk of the tumor as identified by CNV analysis in SNP array data. BAMP: balanced amplification; meaning one copy of each chromosome (maternal/paternal) is gained and no allelic imbalance is detected

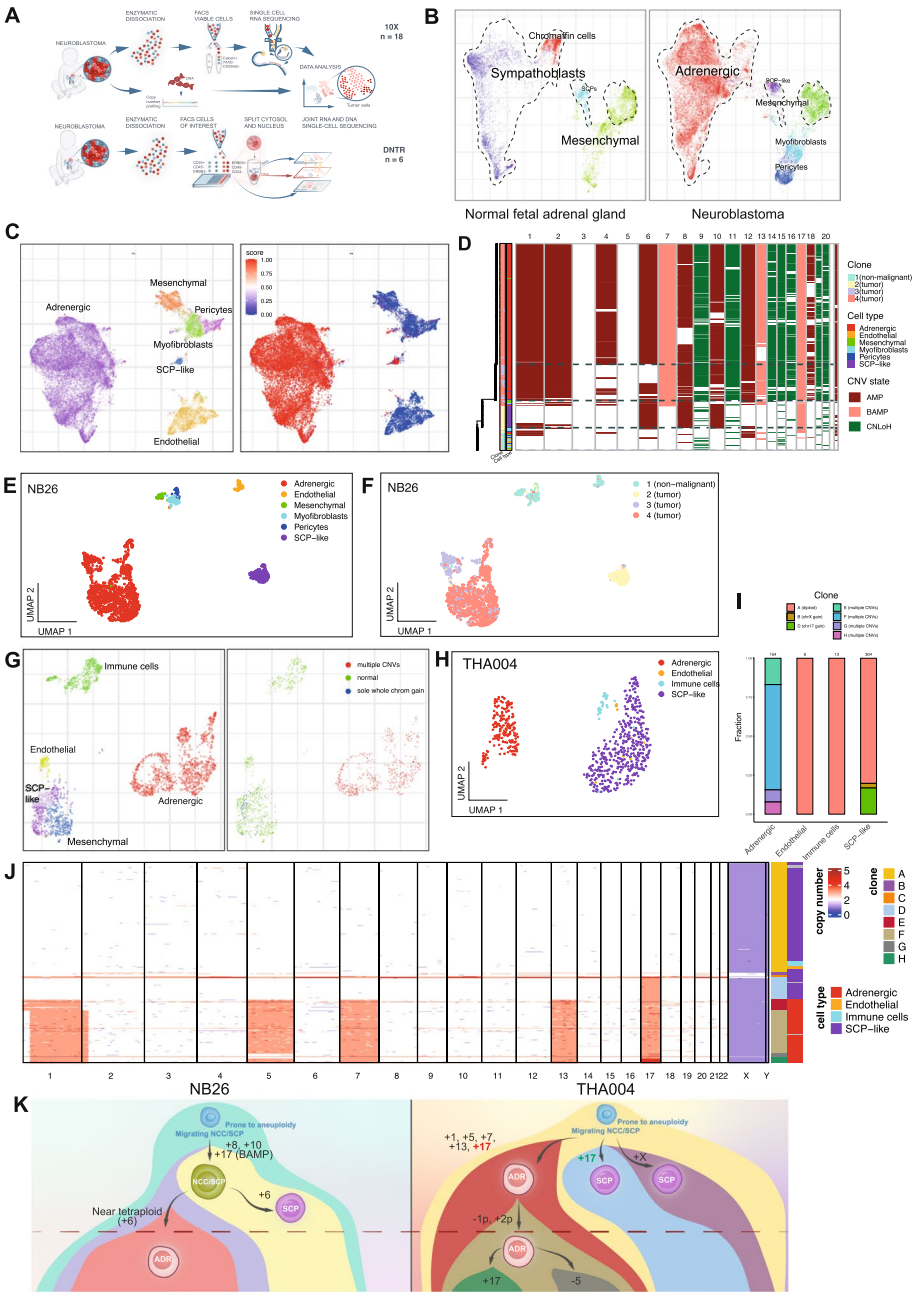

Fig. 1 (See legend on previous page.)

cells without CNVs, while the remaining clones were predicted to be malignant (Fig. 1D-F). Interestingly, clone 2 consisted of SCP-like cells with whole-chromosome gains (+6, +8, +10, and +17). Clones 3 and 4 formed distinct clusters in the UMAP embedding and shared the gain of chromosome 17 with high consistency (Fig. 1D, S1H). The pattern of CNVs in this tumor strongly suggests that clone 2 (SCP-like cells) reflects an early clone in NB development.

Aiming to capture and study the full spectrum of abnormal SCP-like cells in more detail, we characterized 2282 high-quality single cells from six tumor samples using direct nuclear tagmentation and RNA sequencing (DNTR-seq), which allows joint whole genome and transcriptome sequencing of the same single cell (Fig. 1A, S2C, see Methods). We targeted SCP-like cells using the cell surface receptor ERBB3 as a marker (Fig. S2A, S2C).

The identity of targeted cell types was confirmed by the transcriptome of single cells (Fig. 1G; S2D-E, S3A,B).

Adrenergic, mesenchymal, and SCP-like cells of the DNTR-seq dataset expressed the same marker genes as observed in our 10x data (Fig. S2A, B). Distinct SCP-like populations were mainly identified in two samples: THA004 and THA016 (Fig. S2D). Clustering of DNTR-seq data revealed distinct mesenchymal and SCP-like cells directly adjacent each other on the UMAP embedding, indicating transcriptional similarity (Fig. 1G). However, this similarity was sample-specific: in sample THA016, ERBB3$^+$ SCP-like and ERBB3$^-$ MES clusters were clearly distinct (Fig. S3C, D), whereas in sample THA004, they were transcriptionally similar (Fig. S3B, E). As these THA004 ERBB3$^+$ cells expressed SCP/Schwann lineage markers such as *ERBB3, PLP1,* and *CDH19,* and not MES markers such as *PDGFRA, MGP, COL6A3* or *LUM*, we chose to annotate all of them as SCP-like cells (Fig. 1H, S3E).

To identify malignant cells, we generated single-cell CNV profiles from DNTR whole-genome sequencing data (Fig. 1G, S3F). Again, all adrenergic cells were found to carry multiple CNVs which recapitulated SNP array tumor CNV profiles (Fig. 1G, S8B). The SCP and MES clusters of sample THA016 were not found to carry any CNVs (data not shown).

Strikingly, we again observed a low-risk NB sample (THA004, derived from an untreated primary tumor of the left sympathetic side chain; Fig. 2A, Table S1) with a clear SCP-like subclone harboring a sole whole-chromosome 17 gain (clone D; Fig. 1I-J; S3A, F).

In this sample, we discovered seven distinct cellular clones of SCP-like and adrenergic identity (Fig. 1J). The majority of SCP-like cells (Clone A, $n=272$) did not display any CNVs. However, a notable SCP-like subclone (Clone D, $n=53$) carried whole-chromosome 17 gains. Chromosome 17 gain was also observed in all malignant adrenergic cells in the sample (Fig. 1J), suggesting that this subclone of SCP-like cells represents an early clone in this tumor. Besides these abnormal, presumably pre-malignant SCP-like cells, we detected one further aberrant clone within the SCP-like cell population. Clone B ($n=9$) had an additional X chromosome, a genomic aberration that was specific to this clone. Furthermore, we identified malignant adrenergic cells that carried additional whole-chromosome gains besides chromosome 17 (Clone E, $n=24$). Malignant adrenergic cells with a relative loss of chromosome 1p and an additional gain on chromosome 2p (Clone F, $n=109$) reflect the dominant malignant clone in this tumor, as was reflected in the bulk DNA SNP array analysis of this sample (Fig. S8B). We also identified two further adrenergic subclones, including a small subclone carrying an additional copy of chromosome 17 (Clone H: $n=12$; Clone G: $n=15$; Fig. 1J). This presence of multiple malignant subclones indicates ongoing chromosomal instability in the tumor population.

Tumor phylogeny in neuroblastoma with abnormal SCPs

In both samples with abnormal SCPs, the pattern of aberrations compared to adrenergic tumor cells suggests an early-stage origin of the SCP-like NB cells during tumor development, potentially representing ancestral cells from a direct precursor clone to the adrenergic tumor cells. To study this in more detail, we analyzed the potential ancestry of SCP-like cells by incorporating allele-specific CNV information. In particular, we studied chromosomes 6, 8, and 10, since these were imbalanced

(See figure on next page.)

Fig. 2 Abnormal SCP-like cells in neuroblastoma retain key developmental niche traits and display a transcriptomic phenotype related to proliferation and diminished immune regulation. **A** Samples used for scRNAseq and validation experiments. Colors indicate clinical details. **B** Upper panel: Example of abnormal SOX10+ cells (as defined by 3 or more *PPM1D* signals) located in intimate proximity to neurofilament (as defined by NF200 protein). Bottom panel: Quantification of NF200-associated abnormal SOX10+ cells in three NB samples. X axis label indicates total number of abnormal SOX10+ cells evaluated in each sample. **C** Upper panel: Validation of abnormal SOX10+ cells using combined FISH and immunohistochemistry. SOX10 shown in green, *PPM1D* (located at 17q) FISH signal shown in red. Scale bar indicates 10 µm. Lower panel: Quantification of *PPM1D* FISH signal in SOX10+ nuclei in samples NB09b, NB26, and NB20. Legend indicates total number of SOX10+ cells evaluated in each sample. **D** Immunohistochemistry staining for SOX10 (green), the receptor tyrosine kinase erbB-3 (ERBB3; shown in red), and its ligand neuregulin-1 (NRG1, shown in white) in sample NB22. Scale bar indicates 100 µm. **E** Heatmap showing differentially expressed genes in abnormal, NB-associated SCP-like cells (NB26) shown in green; non-malignant, NB-associated SCP-like cells from remaining 10x samples shown in blue; and normal fetal SCPs shown in red. **F** Scatterplot of cell proliferation scores (signature: Gene Ontology term 0008283) in abnormal SCP-like cells (green), non-malignant NB-associated SCP-like cells (blue), and normal fetal SCPs (red). Groups are compared using Wilcoxon rank-sum test. Abnormal SCP-like vs NB-associated SCP-like: adjusted *p* value 0.014; abnormal SCP-like vs fetal SCP: adjusted *p* value 7.0e-49; NB-associated SCP-like vs fetal SCP: adjusted *p* value 1.6e-46. **G** Dot plot showing all differentially expressed genes in ERBB3$^+$ SCP-like cells (DNTR-seq sample THA004) carrying an extra copy of chromosome 17 compared to diploid SCP-like cells. **H** Heatmap showing expression of selected immune-related genes in neuroblastoma and normal fetal adrenal gland datasets. Green: abnormal SCP-like cells, blue: non-malignant NB-associated SCP-like cells, red: normal fetal SCPs. **I** Gene set enrichment analysis (GSEA) of differentially expressed genes in abnormal, pre-malignant NB-associated SCP-like cells (green), non-malignant NB-associated SCP-like cells (blue), and normal fetal SCPs (red). Horizontal bars indicate negative log of *p* value for the indicated GO:BP gene sets. GSEA analysis was performed using the gProfiler tool (https://biit.cs.ut.ee/gprofiler/gost)

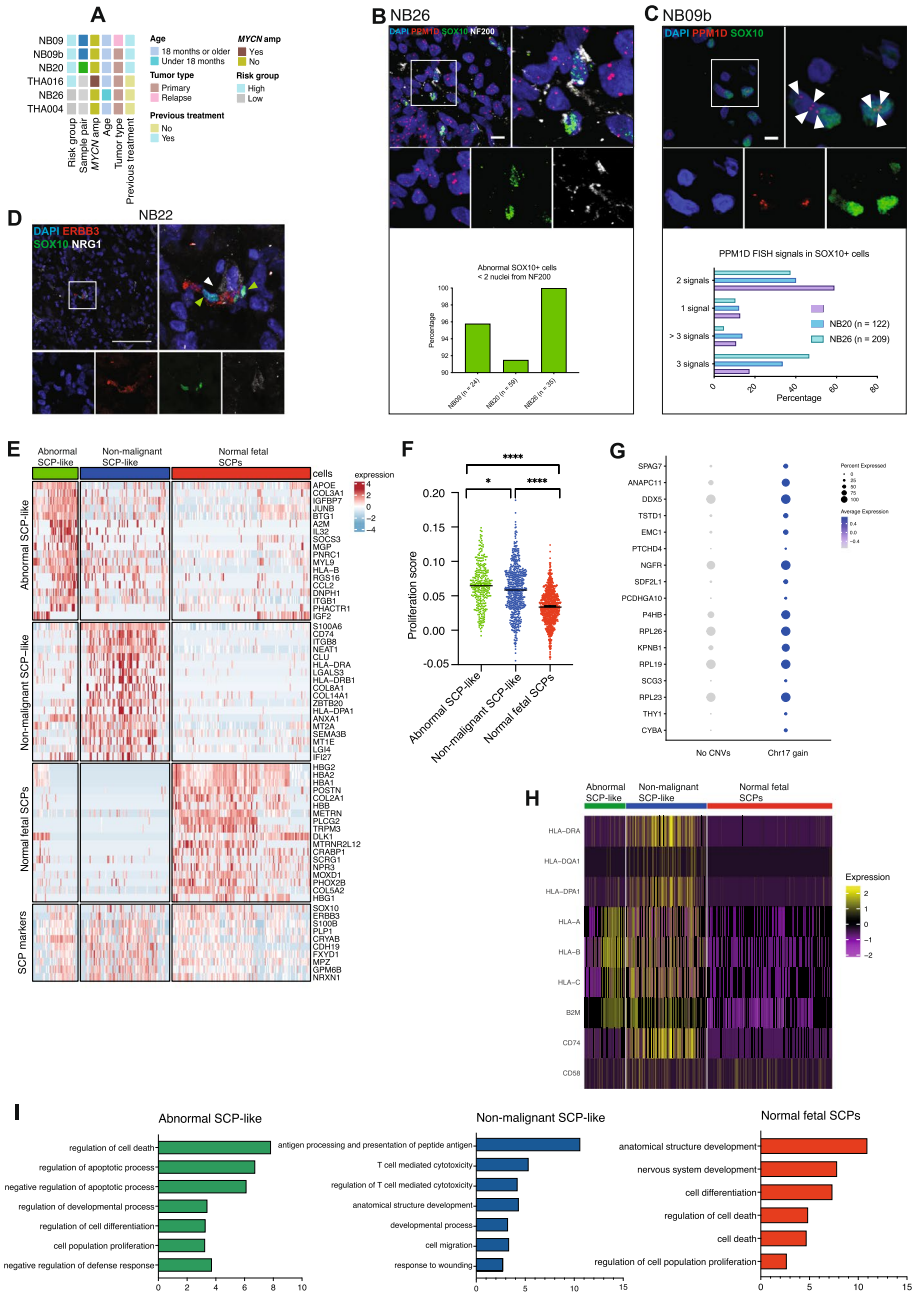

Fig. 2 (See legend on previous page.)

whole-chromosome gains shared by the SCP-like as well as the adrenergic tumor population in NB26 (Fig. 1D; Fig. S4A, B) according to Numbat predictions. Chromosome 17 gain was also shared by SCP-like and adrenergic populations. However, we did not include chr17 in this analysis as there was no allelic imbalance observed in SNP array data, meaning that the tumor carried four chr17 copies – one extra copy of the maternal as well as the paternal chromosome.

We phased alleles into major and minor haplotypes (Supp. Methods) and counted the numbers of these in single cells in order to assess chromosomal imbalance. Chromosome 8 and 10 gains were shared by SCP-like and adrenergic populations. These results indicate that the SCP-like and adrenergic clones share a common ancestor, with gains of chromosomes 8, 10, and 17 as initiating events in tumor development. Chromosome 6 gain was "mirrored", indicating that the opposite chromosomes

were gained in the two populations (Fig. 1K; S4A, B) at a later stage in tumor development.

THA004 displayed shared gains of chromosome 17 in adrenergic tumor and SCP-like populations (Fig. 1J). To resolve the tumor phylogeny of this sample, we assessed chr17 haplotypes in DNTR-seq DNA data based on common germline SNPs (see Methods). Interestingly, we found that the extra chromosome 17 in the SCP-like and adrenergic clones (Fig. S4C, D) are different haplotypes. Thus, the SCP-like cells are unlikely to be direct precursors of the adrenergic tumor cells in this sample, but instead represent parallel clonal evolutions (Fig. 1K). Importantly, the same chromosome 17 haplotype was found in all aberrant SCP-like cells, indicating clonal expansion.

In summary, we identified aneuploid, SCP-like clones in two human NB samples, highlighting the complexity of NB tumor development. These expanding clones share CNVs with adrenergic tumor clones, indicating a pre-malignant state. In sample NB26, this SCP-like clone shares a direct common ancestor with the adrenergic tumor cells, whereas in sample THA004, on the other hand, the SCP-like and malignant adrenergic clones likely represent two "parallel tracks" of tumor development (Fig. 1K).

Validation of abnormal SCP-like cells in neuroblastoma

Next, we sought to validate the presence of karyotypically abnormal SCP-like cells using an orthogonal approach. Specifically, we combined fluorescence in situ DNA hybridization (FISH) targeting chromosome 17 (*PPM1D* locus, 17q23.3) with immunofluorescence protein stainings using SCP transcription factor SOX10 as a marker for SCP-like cells (Fig. 2B-D; S5E-J). Numerical gains of chromosome 17 were identified as a common aberration of pre-malignant SCP-like cells in our analysis. The samples selected for staining all displayed aberrations on 17q as evaluated by SNP array (Fig. 2A, S8).

SOX10+ cells were present in sufficient numbers for FISH signal quantification in three NB samples: NB09b (primary surgery of a pretreated, relapsed tumor, INRGSS: M); NB20, (pretreated, primary adrenal gland tumor, INRGSS: M), and NB26 (INRGSS: L1). In sample NB26, we found that a significant proportion of SCP-like SOX10+ cells carried an extra copy of the *PPM1D* locus, supporting the presence of an extra chromosome 17 copy as inferred from scRNAseq data (Fig. 1D, 2C, S5I). Similar to adrenergic ISL1+ and PHOX2B+ cells harboring an aberrant number of *PPM1D* signals (Fig. S5E, F, H), a fraction of SOX10+ SCP-like cells exhibited an increased and abnormal number of intra-nuclear signals hybridizing to the *PPM1D* locus in all three samples (Fig. 2B, C; Fig. S5I). These shared aberrant *PPM1D* copy numbers between malignant adrenergic and SOX10+ SCP-like cells imply that SCP-like cells may be involved in NB development, and that the SCP-like population likely represents a mixture of abnormal and recruited stromal cells. In conclusion, we detect abnormal SCP-like cells in four different NB using various approaches: DNTR-seq (THA004), combined 10X-scRNAseq and FISH/immunostaining (NB26), and FISH/immunostaining only (NB20, NB09b).

Abnormal SCP-like cells retain their developmental nerve-associated niche

By aligning our scRNAseq data with published data sets from human adrenal gland development, we confirmed the SCP-like identity of NB-associated SCP-like cells (Fig. 1B, S1E). The similarities between normal SCPs of the developing fetus and SCP-like NB cells extended to important functional traits. For instance, using SOX10 as a marker for SCP-like cells, we performed immunostainings to validate the expression and spatial context of SOX10+ cells in NB samples. SOX10 + cells were detected at varying frequencies in all stained samples (Fig. S5 A-D). The migration and differentiation of normal SCPs during development is guided by nerve fibers. The association with the nerves is maintained through the ERBB3 receptor, which in turn binds NRG1 – a critical signal secreted by the nerves [2]. Similar to the SCPs of the developing embryo, the vast majority of SOX10+ cells in NB were positioned close to NF200+ neurofilaments (Fig. S5D). This finding was also observed for abnormal SCP-like cells with additional copies of *PPM1D* as identified in our DNA-FISH staining (Fig. 2B).

SOX10+ cells expressed ERBB3 and the ligand NRG1 was expressed adjacent to SOX10+ cells, indicating that this crucial SCP niche is preserved in NB (Fig. 2D). Some of the neurofilaments resembled recruited nerve bundles, while others appeared diffuse and are likely produced by the adrenergic subpopulation of the tumor cells which also expresses NRG1 (Fig. S2A). Although SCP-like NB cells express many glial genes, with some cells being myelin protein zero (MPZ) positive, most SOX10+ cells do not express the MPZ protein (Fig. S5G). We performed signature scoring analysis on abnormal SCP-like cells, non-malignant NB-associated SCP-like cells and normal fetal SCPs, comparing them to a previously published scRNAseq dataset of the mouse SCP and Schwann lineage (see Methods). SCP-like NB cells were enriched for signatures of non-myelinating and primed Schwann cells (Fig. S5K). These combined results suggest that NB SCP-like cells do not represent a mature Schwann cell phenotype.

Pre-malignant SCP-like cells express gene programs of proliferation, apoptosis and a non-immunomodulatory phenotype

To describe functional differences of the distinct SCP populations, we compared the abnormal SCP-like cells of sample NB26 to non-malignant NB-associated SCP-like cells and normal fetal SCPs (Fig. 2E; Table S4). All three cell types expressed key SCP marker genes such as *SOX10, ERBB3, S100B, PLP1*, and *CDH19* (Fig. 2E). Interestingly, abnormal SCP-like cells exhibited a distinct expression signature with high levels of genes related to regulation of proliferation and apoptosis such as *FOS, JUNB,* and *KLF4* (Fig. 2E; Table S4). Abnormal SCP-like cells also displayed significantly higher proliferation scores (Fig. 2F). Non-malignant, NB-associated SCP-like cells were enriched for gene expression programs related to antigen presentation via MHC class II and T-cell cytotoxicity (e.g. *CD74, B2M, HLA-DRA)* (Fig. 2H). It has previously been described that recruited Schwann cells interact with the immune system after injury and modulate the immune response [5]. Interestingly, we observed that unlike their NB-associated, non-malignant counterparts, abnormal NB-associated SCP-like cells do not express MHC class II genes (*HLA-DRA, HLA-DPA*) (Fig. 2H) and only a subfraction expressed MHC class I molecules *(HLA-A, HLA-B, HLA-C, B2M).* As expected, normal fetal SCPs were characterized by gene expression programs related to nervous system development and cell differentiation (Fig. 2I, Table S5), but also cell death regulation, as an inherent program of developing stem cells. Taken together, these results indicate that abnormal NB-associated SCP-like cells carry a more proliferative, less apoptotic phenotype and do not engage in T-cell interaction and immune regulation.

In sample THA004, abnormal ERBB3^{+} cells harboring an extra copy of chromosome 17 were transcriptionally highly similar to their genomically normal counterparts (Fig. 1G-H, S3A). However, we detected some differentially expressed genes of which the majority are located on chromosome 17. For example, abnormal SCP-like cells showed upregulation of the anaphase complex component gene *ANAPC11,* which is involved in the separation of sister chromatids during cell cycle progression to avoid chromosome segregation errors [9]. Other de-regulated genes include the nerve growth factor receptor gene *NGFR* and the *THY1* cell surface antigen gene (Fig. 2G).

In conclusion, our combined data provide evidence of abnormal, aneuploid SCP-like cells in human NB and further suggest that these cells originate early during tumor development but remain in a hypothetically pre-malignant state with significantly less chromosomal aberrations compared to the adrenergic main tumor population during tumor progression. All pre-malignant SCPs shared whole-chromosome 17 gains, reflecting aneuploidy as a potential tumor-initiating event in NB.

Discussion

In this study we analyzed transcriptomic and genomic heterogeneity of NB at the single-cell level. With our multi-omics approach of single-cell transcriptomics combined with allele-specific transcriptome-based CNV predictions (*Numbat)*, DNTR sequencing and comprehensive DNA FISH/protein stainings, we describe the cellular constitution of NB. We analyzed NB cell phenotypes in relation to fetal cell states and, like others, found that the vast majority of tumor cells resembled fetal sympathoblasts, while a minority of adrenergic tumor cells had a chromaffin-like signature [3]. Importantly, in addition to adrenergic tumor cells, we identified a previously uncharacterized population of abnormal aneuploid cells of a SCP-like cell state.

The role of Schwannian stromal cells in NB has been widely debated [1, 4, 5, 10]. These tumor-associated Schwann cells often display a phenotype similar to that of repair Schwann cells, which is seen after nerve injury. They retain a flexible differentiation state and occur as immature or non-myelinating Schwann cells, which is still a poorly characterized phenotype [11]. In the NB context, one previous study has described that Schwannian cells derive from the same tumor clone as neuroblastic cells, suggesting that they represent differentiated tumor cells [12]. In our current study, the vast majority of Schwannian lineage cells are non-malignant and seem to reflect stroma cells as described by others. They probably also reflect a continuum of differentiation states, from SCP-like to immature and differentiated myelinating Schwann cells. However, we also detected a minor proportion of aneuploid SCP-like cells, some of which were clonally related to adrenergic malignant cells. Besides significant differences in proliferation and apoptosis regulation, the major functional difference between abnormal SCP-like cells and recruited, non-malignant Schwannian stromal cells seems to be the immunoregulatory phenotype. While NB-associated Schwann cells are actively involved in immunoregulation, we found that abnormal SCP-like cells do not express MHC class II molecules or even downregulate MHC class I expression. Although these observations indicate putative roles of SCP-like cells in the NB microenvironment, further studies will be needed in order to assess the functional role of aneuploid SCP-like cells in NB initiation and clonal progression.

In normal development, SCPs are precursors of fetal neuroblasts in a cellular transition assumed to happen during the first trimester of pregnancy [2, 3]. A recent study shed light on the presumed temporal origin of NB based on the allele frequencies of clock-like mutation

signatures in whole-genome sequencing data and concluded that NB originates from proliferating sympathoblasts also during the first trimester of pregnancy [13]. At this stage, a sub-population of fetal intra-adrenal sympathoblasts derive from proliferating and migrating SCPs, raising the possibility that the first oncogenic transformation occurs in SCPs before they differentiate into sympathoblasts [2, 13]. The dynamics of proliferating cell lineages during fetal development and the time of NB onset could explain our findings that abnormal SCP-like cells are very rare and hard to detect. The study by Körber et al. has shown that the earliest cells of tumorigenesis are most likely lost due to cell death or differentiation at the time of sampling or the formation of the "most recent common ancestor" [13]. Interestingly, the model proposed by Körber et al. also suggests that low-risk tumors display less cell loss and hence reach a detectable tumor size earlier than high-risk tumors. This fact might explain why we detected abnormal SCP-like cells in low and medium-risk NB only, while in high-risk tumors the SCPs, if abnormal, might be outcompeted by rapidly dividing adrenergic cells. The genetic constitution of SCP-like cells in sample NB26 and THA004 suggests that one of the first oncogenic hits in these samples were whole-chromosome gains, followed by stepwise acquisition of additional gains. In sample THA004, a subclone of aneuploid tumor cells also gained additional segmental aberrations, indicating aneuploidy as a tumor-driving mechanism of increased chromosomal instability.

Comprehensive single-cell studies of human NB and healthy fetal adrenal tissue have revealed that NB cells resemble sympathoblasts of various differentiation states [2, 3, 6], suggesting a tumor evolution model in which the first tumor cell is a rapidly proliferating fetal sympathoblast that most likely arises during the first trimester of pregnancy [13]. Our data suggest that the first steps of oncogenic transformation can, in some tumors, also happen in migrating fetal SCPs or neural crest cells, before committing to the sympatho-adrenal lineage. The transition of fetal SCPs to early sympathoblasts happens via a fork-like transition along with parallel expression of markers of both lineages [2]. At this stage, proliferating SCPs may be susceptible to chromosomal instability and subsequent clonal selection. These aneuploid multipotent progenitors may then continue their developmental trajectories and further clonal evolution. In human development, pre-malignant SCPs might potentially either differentiate into adrenergic tumor cells acquiring further genomic aberrations, or they remain in an undifferentiated SCP-like state.

In NB, the tumor initiating event is still unknown but, most likely, various molecular mechanisms can potentially induce an oncogenic transformation in precursor cells of the adrenal gland. This process is characterized by ongoing genomic instability in the form of aneuploidy and the acquisition of CNVs [13]. Although the mutational burden is low and recurrent mutations are rare, hereditary NB is often caused by germline mutations in the *ALK* gene, which predispose individuals to NB [1, 8]. When high-risk tumors progress, however, somatically acquired mutations, e.g. in the *ALK* or *RAS* genes together with mechanisms of telomere maintenance, are more frequent and determine the fate of the tumor [6, 8, 13]. Tumorigenesis in NB is highly individual and cannot always be accounted to single driver genes but might be driven by aneuploidy itself [13]. Notably, the presence of segmental chromosomal aberrations is always associated with a high risk of relapse, whereas numerical aberrations alone indicate a good prognosis. The type of aneuploidy, segmental or whole chromosome aberrations, is more relevant to the prognosis than which specific chromosome is affected. Considering the low frequency of somatic mutations, gene dosage effects of multiple genes encoded on affected chromosomes might be driving tumor progression in these NB. The strongest dependency factor in NB is the amplification of the *MYCN* gene. However, some segmental aberrations including 1p deletion, 11q deletion, and 17q gain independently correlate with a worse prognosis in *MYCN*-amplified and non-amplified tumors [1]. In *MYCN*-amplified tumors, 17q gain supports the tumor driving effect of *MYCN* e.g. by an enhanced proliferation of these cells [14]. It is still unknown when those highly recurrent CNVs occur during tumor development but our data support findings by others describing numerical or segmental gains of chromosome 17(q) as an early event [14, 15], possibly also in SCPs during the fetal period.

We propose that in some NB, this initiating aneuploidy occurs in populations of migrating neural crest cells or in SCPs, before lineage commitment to adrenergic cell states. Aneuploid cells may subsequently undergo clonal expansion due to increased fitness. Interestingly, we observed signs of convergent tumor evolution in both samples. In NB26, chromosome 6 gains likely occurred independently in SCP-like and adrenergic clones. Our data from sample THA004 also opens up for the possibility of parallel tumor evolution, with two or more independent clones emerging from the aneuploid-prone progenitors, converging on chromosome 17. The gene-dosage effect of chromosome 17 gain seems particularly beneficial in the sympatho-adrenal lineage. As seen in sample THA004, whole-chromosome 17 gain as a sole CNV is not sufficient to establish a full malignant phenotype, but is a commonly observed event in low-risk NB while segmental chromosome 17q gains are an adverse event in high-risk NB [1]. In abnormal SCP-like cells with

whole-chromosome 17 gain, we identified *ANAPC11* as a significantly de-regulated gene. *ANAPC11* is involved in chromatid separation during cell division and its deregulation might reflect a cause or consequence of initial aneuploidy as the tumor initiating event in NB.

Interestingly, high-risk NBs with a mesenchymal-like cell state share many aspects of the undifferentiated state of SCPs [3, 6, 8]. It has been reported that mesenchymal-like and adrenergic tumor cells share the same genomic aberrations. This suggests that the neural crest or mesenchymal-like phenotype may be acquired via epigenetic changes and key signaling regulators such as the RAS pathway [6]. The mesenchymal-like phenotype usually correlates with high-risk disease, tumor relapse, or therapy resistance; and most likely reflects a cell state acquired through dedifferentiation due to genomic instability and progressive tumor evolution as well as selective treatment pressure [6]. We, however, detected abnormal SCP-like cells in low-risk samples and the SCP-like cells had few genomic aberrations, suggesting that abnormal SCP-like cells occur early in tumor development, remain in their initial cell state, and are not a result of tumor dedifferentiation.

Although the SCP-like cells display certain characteristics of cancer stem cells, they could not be cultured in various preclinical models tested, including cell lines, organoid culturing of primary human NB samples, patient-derived xenografts, and transgenic mouse models (data not shown). This is most likely because SCP-like cells in NB are scarce and pre-malignant. SCPs normally depend on the axon for survival [2] and SCP-like NB cells, which may have acquired a pre-malignant phenotype, are most likely still highly dependent on their niche and cannot be propagated in culture.

A weakness of the study is that we have mostly studied one sampling location in one tumor at a given timepoint. Tumor evolution is a continuous process over time, occurring in billions of tumor cells simultaneously, strongly affected by selective treatment pressure on cells—of which we have only studied a snapshot. Due to the low availability of tissue and surgical specimens, especially from low- and medium-risk tumors, we are unable to draw a complete picture of the role SCPs during tumor progression and under treatment pressure. A more in-depth characterization of abnormal SCPs compared to healthy Schwannian stroma cells requires a broader spectrum of abnormal SCPs from different samples with various clinical characteristics. Clinically relevant tumor heterogeneity likely expands way beyond our observations, and comprehensive understanding will require large international collaborative efforts.

To conclude, our study sheds light on novel aspects of tumor evolution and heterogeneity in NB at unprecedented resolution. Within a subset of NB, we propose that the initiating event of tumor development is aneuploidy and clonal expansion occurring in migrating neural crest cells or SCPs. These putative pre-malignant cells may remain in the microenvironment as the tumor progresses, with diminished immunomodulatory activity compared to Schwannian stroma cells.

Abbreviations

AMP	Amplification / copy number gain
17q	Long arm (q) of chromosome 17
2p	Short arm (p) of chromosome 2
5-TAMRA	5-Carboxytetramethylrhodamine
7AAD	7-Aminoactinomycin D
AF700	Alexa Fluor 700
BAMP	Balanced amplification
CGH	Comparative genomic hybridization
CNLoH	Copy-number neutral loss of heterozygosity
CNV	Copy number variation
DAPI	4′,6-Diamidino-2-phenylindole
DNTR-seq	Direct nuclear tagmentation and RNA sequencing
ENCODE	Encyclopedia of DNA elements
ERCC	Evaluation of External RNA Controls Consortium
FACS	Fluorescence-activated cell sorting
FBS	Fetal bovine serum
FISH	Fluorescence in situ hybridization
GC	Guanine and cytosine
GEO	Gene Expression Omnibus
GO:BP	Gene Ontology: Biological process
GO:CC	Gene Ontology: Cellular component
ILC3	Type 3 innate lymphoid cells
INRGSS	International Neuroblastoma Risk Group Staging System
LLR	Log-likelihood ratio
Mb	Megabase
mDC	Myeloid dendritic cells
MES	Mesenchymal
MHC	Major histocompatibility complex
NB	Neuroblastoma
NK cells	Natural killer cells
PBS	Phosphate-buffered saline
PBST	Phosphate-buffered saline with Tween
PCA	Principal component analysis
PCR	Polymerase chain reaction
pDC	Plasmacytoid dendritic cells
PE	Phycoerythrin
Rpm	Revolutions per minute
SCP	Schwann cell precursors
scRNA-seq	Single-cell RNA sequencing
SNP	Single nucleotide polymorphism
SSC	Saline-sodium citrate buffer
Tcyto	Cytotoxic T cells
Th	T helper cells
Treg	Regulatory T cells
UMAP	Uniform manifold approximation and projection
UMI	Unique molecular identifier

Supplementary Information

The online version contains supplementary material available at https://doi.org/10.1186/s12943-024-02091-y.

Supplementary Material 1: Figure S1. Integrative scRNAseq analysis of NB: sample overview, comparison to normal fetal adrenal gland, and CNV prediction using Numbat. **A** Overview of all samples included in the study labelled according to risk group, genetic profile, age, anatomical site, tumor type (primary / recurrent) and whether the child had received therapy prior to surgery/biopsy. Samples are also labelled according to the method(s) applied. **B** Pie chart showing the fraction of cells that each

sample contributed to the full 10x dataset. **C** Barplot representing the fraction of major cell type within each sample (10x dataset). B: B lymphocytes; ILC3: type 3 innate lymphoid cells; mDC: myeloid dendritic cells; NK: natural killer cells; pDC: plasmacytoid dendritic cells; Tcyto: cytotoxic T cells; Th: T helper cells; Treg: regulatory T cells. **D** Integrative analysis of scRNAseq data (10x dataset) from 18 neuroblastoma samples, visualized using a common UMAP embedding. Left panel: Individual samples. Right panel: Major cell populations. Treg: regulatory T cells, Th: T helper cells, Tcyto: cytotoxic T cells, NK: natural killer cells, ILC3: type 3 innate lymphoid cells, pDC: plasmacytoid dendritic cells, mDC: myeloid dendritic cells, B: B lymphocytes. **E** Correlation of the overall expression profiles between different neuroblastoma and fetal adrenal cell types, illustrating best matching cell populations. **F** High level of concordance between single-cell (RNA) and bulk (DNA) CNV detection, exemplified by sample NB13. Top panel: Pseudobulk CNV profile of sample NB13 from Numbat analysis. Green color indicates copy-neutral loss of heterozygosity (cnLOH), red color indicates copy number gain, blue color indicates copy number loss; light red/pink color indicates balanced amplification (BAMP; i.e CNV without allelic imbalance). Bottom panel: CNV profile from bulk DNA SNP array analysis of the same sample. **G** Individual UMAP embeddings of NB samples (10x dataset). Top panel: Cells labelled by Numbat's predicted joint posterior CNV score ("malignancy score"). Red color indicates high probability of CNVs in the cell; blue color indicates low CNV probability. Bottom panel: Cells labelled by cell type. Aneuploid SCP-like cells in sample NB26 are marked with a black arrow in both panels. **H** Numbat pseudobulk profiles of CNVs in sample NB26, clones 2-4. Clones correspond to those shown in Fig. 1D.

Supplementary Material 2: Figure S2. ERBB3 and CD24 enrichment enables capture of SCP-like, mesenchymal, and adrenergic neuroblastoma populations. **A** Expression of select marker genes in adrenergic, mesenchymal, and SCP-like populations (10x dataset). **B** Expression of select marker genes in adrenergic, mesenchymal, and SCP-like populations (DNTR-seq dataset); genes correspond to those shown in panel A). **C** Gating strategy for DNTR-seq cell sorting; exemplified by FACS data from sample THA004. Single live cells were gated according to CD45, ERBB3, and CD24 signal. **D** Left panel: Integrative analysis of DNTR-seq RNA data ($n = 5$), common UMAP embedding, only cells from individual samples are shown in each plot. Middle panel: Integrative analysis of DNTR-seq RNA data, clustering-based annotation. Right panel: Integrative analysis of DNTR-seq RNA data, cells labelled according to label transfer from 10x dataset. **E** Integrative analysis of scRNAseq data from DNTR-seq RNA ($n = 5$) and 10x ($n = 18$) datasets, common UMAP embedding, labelled by cell type. Left panel: Cells from 10x dataset, labelled according to cell type. Right panel: Cells from DNTR-seq dataset, labelled according to cell type.

Supplementary Material 3: Figure S3. Sample-specific annotation of SCP-like and MES cells in DNTR-seq data; summary of CNV detection per cell type and sample. **A** UMAP of DNTR-seq sample THA004, labelled by clone. Clones correspond to those shown in Fig. 1J. **B** UMAP of DNTR-seq sample THA004, labelled by surface protein expression (FACS). Adrenergic cells (left cluster) are $CD24^+$, $CD45^-$. SCP-like cells (right cluster) are $ERBB3^+$, $CD45^-$. **C** UMAP of DNTR-seq sample THA016, labelled by cell type. **D** Heatmap showing expression of adrenergic, SCP-like, and mesenchymal marker genes in THA016 DNTR-seq sample; cells downsampled to $n = 42$ per group. **E** Heatmap showing expression of adrenergic, SCP-like, and mesenchymal marker genes in THA004 DNTR-seq sample, in all $ERBB3^+$ cells, grouped by original cluster-based annotation. All $ERBB3^+$ cells display similar expression pattern with expression of SCP-like markers but no consistent expression of mesenchymal markers. **F** Bar plot showing fractions of CNVs in DNTR-seq dataset. Adrenergic cells consistently carry multiple CNVs in all samples, whereas immune, endothelial, and mesenchymal cells are diploid. SCP-like cells carry sole whole-cromosome gains in sample THA004 but are diploid in sample THA016.

Supplementary Material 4: Figure S4. Haplotype-specific analyses of aneuploid SCP-like cells. **A** Allelic frequencies from SNP array data, sample NB26. BAF: B allele frequency. **B** Major haplotype frequency on chromosomes 6, 8, and 10 in different cell populations of sample NB26. Horizontal blue line indicates balanced allelic proportion (0.5). Error bars represent 95% confidence intervals from a binomial distribution. Multiple testing correction was performed using the BH correction. **C** Fraction of one haplotype "Haplotype A" across chromosome 17. Lines are running mean of haplotype A fraction across, $k = 200$. **D** Beeswarm plot showing chromosome-wide mean of the haplotype gained in the tumor clone. Fractions were calculated for each cell individually.

Supplementary Material 5: Figure S5. Immunostaining and FISH of human NB samples; transcriptional characterization of functional traits in SCP-like NB cells. **A** Immunohistochemistry stainings for SOX10 (shown in green) demonstrating variations in SOX10+ abundance between samples. The region enlarged in the right panel is marked by the white square in the left panel. **B** Quantification of SOX10+ cells per 1000 nuclei in seven neuroblastoma samples. Total number of DAPI+ nuclei ranged from 2518 (sample NB09b) to 11002 (sample NB26). Cells on 3-7 tile scans were included in the calculation. **C** Immunohistochemistry staining for neurofilament 200 (NF200; shown in red) and SOX10 (shown in green) on a section from sample NB20. SOX10+ nuclei are situated in close proximity to NF200 protein. Scale bar indicates 100 µm. **D** Percentage of SOX10+ cells located at a distance of 0-2 nuclei from NF200 protein; quantification in seven neuroblastoma samples. **E** and **F** Validation of malignant adrenergic ISL+ cells using combined FISH and immunohistochemistry in samples NB24 (E) and NB09b (F). *PPM1D* FISH signal shown in red, ISL1 protein signal shown in white. Scale bar indicates 10 µm. Orange arrows indicate aberrant number of *PPM1D* copy numbers in ISL1+ neuroblastoma cells. **F G** Immunohistochemistry staining for neurofilament 200 (red), SOX10 (green), and myelin protein zero (MPZ; yellow) in sample NB09b. Most SOX10+ cells do not express MPZ. Scale bar indicates 100 µm. **G H** Validation of malignant adrenergic PHOX2B+ cells using combined FISH and immunochemistry in sample NB26. Left panel: *PPM1D* FISH signal shown in red; PHOX2B protein signal shown in cyan. Scale bar indicates 10 µm. Orange arrows indicate a cell with three *PPM1D* copies; white arrows indicate a cell with four *PPM1D* copies. Right panel: Manual quantification of *PPM1D* signal in PHOX2B+ adrenergic cells in sample NB26. **H I** Automated quantification of *PPM1D* FISH signal in sample NB26. SOX10+ as well as SOX10- cells display abnormal subpopulations of cells with 3 or more *PPM1D* signals. **I J** Example image of automated quantification of *PPM1D* FISH signal in sample NB26. Right upper panel: automated identification and numbering of nuclei based on DAPI staining. Lower panels: zoom-in of a SOX10+ cell carrying three *PPM1D* signals. **J K** Signature score analysis of abnormal/aneuploid (green) and non-malignant (blue) NB-associated SCP-like cells as well as normal fetal SCPs (red) according to previously published expression signatures of mouse neural crest, SCP, and Schwann lineage cell states (Kastriti et al, see Methods).

Supplementary Material 6: Figure S6. Numbat single-cell CNV calls and predicted phylogeny; all cell types included in the analysis. Left annotation bar indicates genotype (i.e. clone) where clone 1 are predicted to be normal without any CNVs. Right annotation bar indicates cell type. Cells above horizontal dashed line are predicted as tumor.

Supplementary Material 7: Figure S7. Numbat tumor/normal predictions; all cell types included in the analysis. UMAPs of individual neuroblastoma samples labelled by genotype (clone). Clone 1 cells (red) are predicted to be normal without CNVs. Genotype corresponds to that shown in Fig. S6. Adrenergic, mesenchymal, and SCP-like populations are highlighted.

Supplementary Material 8: Figure S8. CNV profiles from bulk DNA SNP array analysis. **A** Results in 10x dataset samples. **B** Results in DNTR-seq dataset samples.

Supplementary Material 9. Supplementary Table S1. Patient and sample characteristics.

Supplementary Material 10.Supplementary Table S2. Marker genes used for cell annotation.

Supplementary Material 11. Supplementary Table S3. Sequencing metrics; cellranger output (v7.0).

Supplementary Material 12. Supplementary Table S4. Differentially expressed genes in NB26 abnormal SCPs ("Abnormal SCP", NB-associated non-malignant SCP-like cells ("SCP-like"), and normal fetal SCPs.

Supplementary Material 13. Supplementary Table S5. Gene set enrichment analysis (GO:BP gene set) of differentially expressed genes in abnormal SCP-like, non-malignant SCP-like, and normal fetal SCP populations. Output from g:Profiler analysis (see Methods).

Authors' contributions

Conceptualization, N.B.; Investigation, T.K.O., J.O., S.M., B.E., H.C, V.Z, I.A., J.I.J., J.S., E.S., M.E., P.Ka., P.Ko., P.V.K. and N.B.; Validation, T.K.O., J.O., P.Ka., B.E., E.K., T.M., S.F., S. S. F., I. T.; Computational investigation and analysis, T.K.O., S.M., T.G., V.Z., Å.B., Z.H., A.J., and P.V.K.; Writing – Original draft, T.K.O., J.O., B.E., I.A., P.V.K. and N.B.; Writing – Review & Editing, T.K.O., J.O. E.S., I.A., J.I.J., P.Ko., M.E., P.V.K. and N.B.; Funding Acquisition, Resources & Supervision, M.E., P. Ko., P.V.K., and N.B.

Funding

T.K.O was funded by the Wenner-Gren Foundation, the Swedish Childhood Cancer Fund, and Mary Bevé foundation. J.O. was funded by the Swedish Childhood Cancer Fund. N.B. was funded by the Swedish Childhood Cancer Fund, the Swedish Cancer Society, Swedish Research Council, Jaenssons stiftelse and Research Funds of Radiumhemmet. P.Ko. was funded by the Swedish Research Council, the Swedish Childhood Cancer Fund, and the Swedish Foundation for Strategic Research. T.K.O, N.B., P.Ko., Å.B., and A.J. were financially supported by the Knut and Alice Wallenberg Foundation as part of the National Bioinformatics Infrastructure Sweden at SciLifeLab. I.A. was supported by ERC Synergy grant (KILL-OR-DIFFERENTIATE), Swedish Research Council, Paradifference Foundation, Bertil Hallsten Research Foundation, Cancer Foundation in Sweden, Knut and Alice Wallenberg Foundation, Austrian Science Fund (FWF) project grant and SFBF78 consortium funding. P.V.K. was founded by the NSF-14–532-CAREER grant.

Availability of data and materials

10x single-cell RNA-seq, DNTR-seq and array CGH datasets are available at the Gene Expression Omnibus (GEO) portal; accession numbers: GSE147766, GSE147773, GSE261828. All other data needed to evaluate the conclusions in the paper are available within the main text or supplementary materials.

Declarations

Ethics approval and consent to participate

Neuroblastoma samples from Swedish children were collected after parents or guardians had given consent according to ethical permits (Regional Ethics Committee in Stockholm; reference 03–736, 2009/1369–31/1, 2022–07254-01). Clinical data were obtained from hospital records according to the ethical permit.

Competing interests

Peter Kharchenko declares that he is an employee of Altos Labs. All other authors declare no conflict of interest.

Author details

[1]Department of Women's and Children's Health, Childhood Cancer Research Unit, Karolinska Institutet, Stockholm 171 77, Sweden. [2]Department of Immunology, Genetics, and Pathology, Uppsala University, Uppsala 752 36, Sweden. [3]Department of Biomedical Informatics, Harvard Medical School, Boston, MA 02115, USA. [4]St. Anna Children's Cancer Research Institute (CCRI), Vienna, Austria. [5]Department of Oncology-Pathology, Karolinska Institutet, Stockholm 171 77, Sweden. [6]National Bioinformatics Infrastructure Sweden, SciLifeLab, Uppsala University, Uppsala 752 36, Sweden. [7]Department of Ophthalmology, Schepens Eye Research Institute of Massachusetts, Eye and Ear, Boston, MA 02115, USA. [8]Department of Ophthalmology, Harvard Medical School, Boston, MA 02115, USA. [9]Department of Neurobiology, Care Sciences and Society, Division of Neurogeriatrics, Karolinska Institutet, Stockholm 171 77, Sweden. [10]Department of Laboratory Medicine, The Sahlgrenska Academy, University of Gothenburg, Sahlgrenska University Hospital, Gothenburg 413 45, Sweden. [11]Department of Physiology and Pharmacology, Karolinska Institutet, Stockholm 171 77, Sweden. [12]Department of Neuroimmunology, Center for Brain Research, Medical University Vienna, Vienna 1090, Austria. [13]San Diego Institute of Science, Altos Labs, San Diego, CA 94022, USA.

Received: 18 May 2024 Accepted: 15 August 2024
Published online: 31 August 2024

References

1. Matthay KK, Maris JM, Schleiermacher G, Nakagawara A, Mackall CL, Diller L, Weiss WA. Neuroblastoma Nat Rev Dis Primers. 2016;2:16078. https://doi.org/10.1038/nrdp.2016.78.
2. Kameneva P, Artemov AV, Kastriti ME, Faure L, Olsen TK, Otte J, Erickson A, Semsch B, Andersson ER, Ratz M, et al. Single-cell transcriptomics of human embryos identifies multiple sympathoblast lineages with potential implications for neuroblastoma origin. Nat Genet. 2021;53:694–706. https://doi.org/10.1038/s41588-021-00818-x.
3. Jansky S, Sharma AK, Korber V, Quintero A, Toprak UH, Wecht EM, Gartlgruber M, Greco A, Chomsky E, Grunewald TGP, et al. Single-cell transcriptomic analyses provide insights into the developmental origins of neuroblastoma. Nat Genet. 2021;53:683–93. https://doi.org/10.1038/s41588-021-00806-1.
4. Weiss T, Taschner-Mandl S, Janker L, Bileck A, Rifatbegovic F, Kromp F, Sorger H, Kauer MO, Frech C, Windhager R, et al. Schwann cell plasticity regulates neuroblastic tumor cell differentiation via epidermal growth factor-like protein 8. Nat Commun. 2021;12:1624. https://doi.org/10.1038/s41467-021-21859-0.
5. Zhang SH, Shurin GV, Khosravi H, Kazi R, Kruglov O, Shurin MR, Bunimovich YL. Immunomodulation by Schwann cells in disease. Cancer Immunol Immunother. 2020;69:245–53. https://doi.org/10.1007/s00262-019-02424-7.
6. Gartlgruber M, Sharma AK, Quintero A, Dreidax D, Jansky S, Park YG, Kreth S, Meder J, Doncevic D, Saary P, et al. Super enhancers define regulatory subtypes and cell identity in neuroblastoma. Nat Cancer. 2021;2:114–28. https://doi.org/10.1038/s43018-020-00145-w.
7. Dong R, Yang R, Zhan Y, Lai HD, Ye CJ, Yao XY, Luo WQ, Cheng XM, Miao JJ, Wang JF, et al. Single-Cell Characterization of Malignant Phenotypes and Developmental Trajectories of Adrenal Neuroblastoma. Cancer Cell. 2020;38(716–733): e716. https://doi.org/10.1016/j.ccell.2020.08.014.
8. Zeineldin M, Patel AG, Dyer MA. Neuroblastoma: When differentiation goes awry. Neuron. 2022;110:2916–28. https://doi.org/10.1016/j.neuron.2022.07.012.
9. Zhou Z, He M, Shah AA, Wan Y. Insights into APC/C: from cellular function to diseases and therapeutics. Cell Div. 2016;11:9. https://doi.org/10.1186/s13008-016-0021-6.
10. Ambros IM, Zellner A, Roald B, Amann G, Ladenstein R, Printz D, Gadner H, Ambros PF. Role of ploidy, chromosome 1p, and Schwann cells in the maturation of neuroblastoma. N Engl J Med. 1996;334:1505–11. https://doi.org/10.1056/NEJM199606063342304.
11. Jessen KR, Mirsky R, Lloyd AC. Schwann Cells: Development and Role in Nerve Repair. Cold Spring Harb Perspect Biol. 2015;7: a020487. https://doi.org/10.1101/cshperspect.a020487.
12. Mora, J., Nk, C., Juan, G., Illei, P., Cheung, I., Akram, M., Chi, S., Ladanyi, M., Cordon-Cardo, C., and Gerald, W.L. (2001). Neuroblastic and Schwannian stromal cells of neuroblastoma are derived from a tumoral progenitor cell. Cancer Res. Cancer Res. 2001;61(18):6892–8.
13. Korber V, Stainczyk SA, Kurilov R, Henrich KO, Hero B, Brors B, Westermann F, Hofer T. Neuroblastoma arises in early fetal development and its evolutionary duration predicts outcome. Nat Genet. 2023;55:619–30. https://doi.org/10.1038/s41588-023-01332-y.
14. Saldana-Guerrero IM, Montano-Gutierrez LF, Boswell K, Hafemeister C, Poon E, Shaw LE, Stavish D, Lea RA, Wernig-Zorc S, Bozsaky E, et al. A human neural crest model reveals the developmental impact of neuroblastoma-associated chromosomal aberrations. Nat Commun. 2024;15:3745. https://doi.org/10.1038/s41467-024-47945-7.
15. Gisselsson D, Lundberg G, Ora I, Hoglund M. Distinct evolutionary mechanisms for genomic imbalances in high-risk and low-risk neuroblastomas. J Carcinog. 2007;6:15. https://doi.org/10.1186/1477-3163-6-15.

Publisher's Note